Anisotropic anomalous diffusion modulated by log-periodic oscillations

L. Padilla,[*] H. O. Mártin,[†] and J. L. Iguain[‡]

Instituto de Investigaciones Físicas de Mar del Plata (IFIMAR) and Departamento de Física FCEyN,
Universidad Nacional de Mar del Plata, Deán Funes 3350, AR-7600 Mar del Plata, Argentina

We introduce finite ramified self-affine substrates in two dimensions with a set of appropriate hopping rates between nearest-neighbor sites where the diffusion of a single random walk presents an anomalous *anisotropic* behavior modulated by log-periodic oscillations. The anisotropy is revealed by two different random-walk exponents ν_x and ν_y in the x and y directions, respectively. The values of these exponents as well as the periods of the oscillations are obtained analytically and confirmed by Monte Carlo simulations.

I. INTRODUCTION

The underlying mechanisms of anomalous diffusion on fractal structures have attracted the attention of scientists for many years; see, for example, Ref. [1] and references therein. In this regard, it has been recently found that on some kind of self-similar substrates, in addition to the well-known subdiffusive behavior, the mean-square displacement of a random walk (RW) is modulated by logarithmic periodic oscillations [2–4]. The same kind of modulation was also observed in biased diffusion on random systems [5], earthquake dynamics [6], escape probabilities in chaotic maps [7], processes on random quenched and fractal media [8], diffusion-limited aggregates [9], growth models [10], and stock markets [11]. There is general agreement that this ubiquitous phenomenon appears because of an inherent self-similarity [12] responsible for a discrete scale invariance [13]. Nevertheless, this self-similarity has to be identified for every system.

The origin of log-periodic modulation can be easily determined for a minimal model of RW introduced in Ref. [3]. This model, which depends on two parameters, $L \in \mathbb{N}$ and $0 < \delta \in \mathbb{R}$, consists of a one-dimensional lattice and a single particle moving by jumps between nearest-neighbor (NN) sites. The hopping rates are defined in a way that a region of size L^n (with $n = 0,1,2,\dots$) is characterized by a diffusion coefficient $D^{(n)}$, and the ratio between any two consecutive coefficients is a constant, i.e., $D^{(n+1)}/D^{(n)} = \delta$ for all $n \in \mathbb{N}$. As a result, the RW mean-square displacement is modulated by log-periodic oscillations, and both the RW exponent and the period of the oscillations can be obtained using rather simple arguments and calculations (for more details, see Ref. [3]).

This method can also be applied to the study of a RW on a self-similar substrate in two dimensions. It has been shown [4] that, in this case, each region of size $L^n \times L^n$ (L is the basic length of the substrate, and $n = 0,1,2,\dots$) is characterized by a diffusion coefficient $D^{(n)}$. Here again, a subdiffusive behavior modulated by log-periodic oscillations arises because the ratio $D^{(n+1)}/D^{(n)}$ takes a constant value. It is the symmetry between x and y directions, allowing the heuristic arguments used in the one-dimensional case to be easily generalized to calculate the

values of the RW exponents and the periods of the oscillations. The important point is that, for a particle in a central square of size $L^n \times L^n$, the typical time to leave this square along the x direction is the *same* as that along the y direction.

In this paper we investigate single-particle diffusion on self-affine fractal structures in two space dimensions [14], which are natural extensions of the above-mentioned self-similar fractals. Typical examples of physical systems in which our analysis may be relevant are those related to transport properties of self-affine media, such as diffusion-limited aggregation clusters in a finite strip [15], structures grown with the dielectric-breakdown model in a cylinder [16], and rough fracture surfaces [17].

In general, the lack of symmetry between the two main directions (x and y) makes the analytical treatment difficult. However, the problem simplifies considerably for a special kind of substrate, that in which the space explored by a RW grows with the same anisotropy as the substrate itself does. We study this case first. The same kind of arguments employed to analyze diffusion on self-similar substrates allows us to show that, in this case, the mean-square displacement as a function of time is a power law modulated by log-periodic oscillations, but in contrast with its self-similar analog, the specific properties of this function are now direction dependent. Indeed, although the period of the modulation is isotropic, two different RW exponents exist, one for the displacement in the x direction and another for the displacement in the y direction. We compute analytically the RW exponents and the period of the modulating oscillation and confirm these results by Monte Carlo simulations.

For the sake of completeness, we then study numerically the RW behavior on a more general self-affine substrate. The outcomes of these simulations suggest that, also here, the mean-square displacements along the x and y directions as a function of time follow log-periodic modulated power laws, which are independent of each other.

II. ANALYTICAL APPROACH

We study the behavior of a RW on two self-affine substrates, referred to in what follows as model I and model II. For convenience, each substrate is built in stages. The result of every stage, called a *generation*, is a periodic array of basic or unit cells, consisting of sites connected by bonds. We denote by L_x and L_y the linear size of the unit cell of the first generation

---
[*]lorenapadilla.r@gmail.com
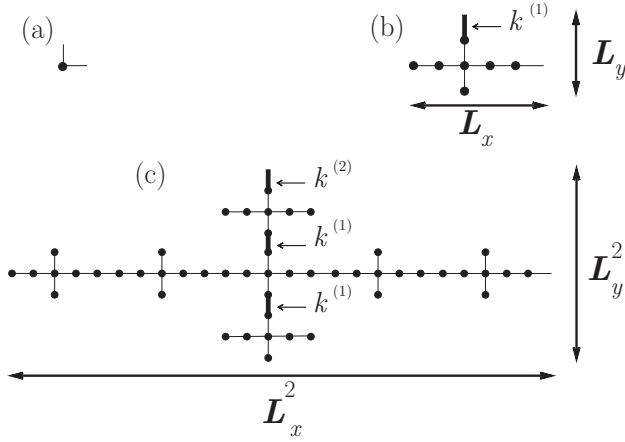[†]hmartin@mdp.edu.ar
[‡]iguain@mdp.edu.ar

FIG. 1. The unit cells of model I. The zeroth, first, and second generation are drawn in (a), (b), and (c), respectively. The basic length scales are $L_x = 5$ and $L_y = 3$. A thin bond (thick bond) represents a hopping rate $k^{(0)}$ ($k^{(i)}$, $i \geqslant 1$). See the text for more details.

in the x and y directions, respectively. Note that this is not a dynamical process but a systematic way to define a full self-affine structure: the nth generation when n goes to infinity (see below). On these substrates the motion of a single particle occurs stochastically. At every time step, the particle jumps with a nonzero probability only between NN sites which are connected by a bond. The details of the models are given in what follows.

A. Model I

The building process is illustrated in Fig. 1, which shows the unit cell for the zeroth, first, and second generations. It is easy to see that, for this model, $L_x = 5$ and $L_y = 3$, where the length unit is the distance between NN sites. It is also apparent from this figure that the second-generation unit cell has linear sizes L_x^2 and L_y^2 in the x and y directions, respectively, and is built from the first-generation one in a self-affine way. In general, the linear sizes of the nth-generation unit cell are L_x^n and L_y^n, and the corresponding two-dimensional periodic substrate is obtained by connecting these cells. (The first-generation substrate is sketched at the top of Fig. 2.)

The full self-affine substrate we are interested in is the result of an infinite number of iterations. Note that this substrate is finitely ramified and that a region of size $L_x^n \times L_y^n$ can be separated from the rest by cutting four bonds.

The hopping rate between any NN connected sites in the x direction is always $k^{(0)}$. On the other hand, the hopping rate in the y direction depends on the site and on the generation. Their values are determined by asking that the mean time to leave a nth-generation unit cell along the x and y directions coincides. We call $t^{(n)}$ this escape time. Because of this constraint, there will be $n + 1$ different hopping rates ($k^{(i)}$, $i = 0, \ldots, n$) related to the nth generation. As an example, in Fig. 1 we show schematics of the zeroth, first, and second generations with one, two, and three kinds of hopping rates, respectively. In this sketch, a thin bond represents $k^{(0)}$ while the other hopping rates are represented by thicker bonds. We can observe that
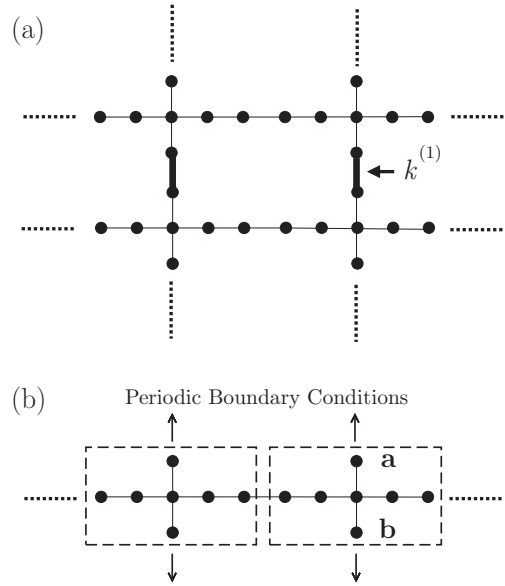

FIG. 2. First generation of model I. (a) The substrate built with the basic cell shown in Fig. 1(b). (b) The infinite one-dimensional string of cells used to compute the diffusion coefficient $D_y^{(1)}$. The arrows indicate periodic boundary conditions in the y direction. For example, if a RW at site **a** (**b**) jumps upward (downward) with a hopping rate $k^{(1)}$, it arrives at site **b** (**a**).

$k^{(1)}$ appears at the top of the first-generation unit cell and $k^{(2)}$ appears at the top of the second-generation one.

We proceed now to analyze the behavior of the diffusing particle on a nth-generation substrate. It is useful to remember that, on any periodic substrate, normal diffusion should be observed if time is long enough for the RW to be influenced by the structure periodicity. As we work with an asymmetric substrate (i.e., $L_x^n \neq L_y^n$ for the nth-generation), we have to consider the x and y directions separately. For the nth-generation substrate, a diffusion coefficient $D_x^{(n)}$ ($D_y^{(n)}$) in the x (y) direction can be defined through the time dependence of the mean-square displacement $\Delta^2 x(t) = \langle [x(t) - x(0)]^2 \rangle$ $\{\Delta^2 y(t) = \langle [y(t) - y(0)]^2 \rangle\}$, i.e., via the relations

$$\Delta^2 x(t) = 2D_x^{(n)} t \tag{1}$$

and

$$\Delta^2 y(t) = 2D_y^{(n)} t, \tag{2}$$

valid for a time t longer than $t^{(n)}$.

The diffusion problem is trivial on the zeroth-generation substrate. This is a simple square lattice, and

$$D_x^{(0)} = D_y^{(0)} = k^{(0)}. \tag{3}$$

The first-generation substrate [see Fig. 2(a)] presents a more difficult task. However, regarding diffusion in the x direction, the whole substrate and the string of cells displayed at the bottom of the same figure with periodic boundary conditions in the y direction lead to equivalent problems. We exploit this equivalence and calculate the diffusion coefficient of that one-dimensional array, following the steady-state method [18]. We get

$$D_x^{(n)} = \left(\tfrac{5}{7}\right)^n k^{(0)}, \quad \text{for } n = 0, 1, 2, \ldots, \tag{4}$$

and thus,

$$D_x^{(n)}\big/ D_x^{(n+1)} = \delta_x = 7/5, \quad \text{for } n = 0,1,2,\ldots. \quad (5)$$

To find the diffusion coefficients in the case of the y direction, we divide Eq. (2) by Eq. (1), imposing the *same escape time* constraint, i.e., $\Delta^2 x(t^{(n)}) = L_x^{2n}$ and $\Delta^2 y(t^{(n)}) = L_y^{2n}$. This leads to

$$\frac{D_y^{(n)}}{D_x^{(n)}} = \frac{L_y^{2n}}{L_x^{2n}} \quad (6)$$

from which the diffusion coefficients

$$D_y^{(n)} = \left(\tfrac{9}{35}\right)^n k^{(0)}, \quad \text{for } n = 0,1,2,\ldots, \quad (7)$$

can be obtained [using Eq. (4) and the values of L_x and L_y]. Hence, the ratio between consecutive coefficients is also a constant in the y direction:

$$D_y^{(n)}\big/ D_y^{(n+1)} = \delta_y = 35/9, \quad \text{for } n = 0,1,2,\ldots. \quad (8)$$

At this stage, the model is completely defined, and the hopping rates are obtained recursively from Eq. (5) by using the above-mentioned trick of converting the two-dimensional diffusion problem into a one-dimensional one:

$$\frac{k^{(n)}}{k^{(0)}} = \left\{ L_x^n - \left[L_y L_x^{n-1} - \frac{k^{(0)}}{k^{(n-1)}} \right] \right\}^{-1}, \quad \text{for } n = 1,2,3,\ldots. \quad (9)$$

Let us now consider a RW on the full self-affine structure. For a time t in the interval $[t^{(n)}, t^{(n+1)}]$, the following relations hold:

$$L_x^n \lesssim \sqrt{\Delta^2 x(t)} \lesssim L_x^{n+1}, \quad (10)$$

$$L_y^n \lesssim \sqrt{\Delta^2 y(t)} \lesssim L_y^{n+1}, \quad (11)$$

and it will be impossible for the RW to distinguish the full self-affine structure from the nth-generation one. Thus, Eqs. (1) and (2) account for the RW behavior in that time window, and the mean-square displacement should behave qualitatively as sketched in Fig. 3. This behavior is reminiscent of single-particle diffusion on a self-similar substrate, whose mean-square displacement as a function of time obeys a log-periodic modulated power law [4]. Because of the lack of symmetry between the x and the y directions, to describe diffusive behavior in the case of a self-affine substrate, we need not one but two functions, which we expect to be

$$\Delta^2 x(t) = C_x t^{2\nu_x} f_x(t) \quad (12)$$

and

$$\Delta^2 y(t) = C_y t^{2\nu_y} f_y(t), \quad (13)$$

where C_x and C_y are constants, ν_x and ν_y are the RW exponents, and $f_x(t)$ and $f_y(t)$ are log-periodic functions with periods τ_x and τ_y, respectively.

The values of these quantities can be computed from the parameters of the model after simple geometrical analysis of Fig. 3 (see the figure caption and Refs. [3,4] for further details). The results are

$$\nu_x = \frac{1}{2 + \frac{\log_{10} \delta_x}{\log_{10} L_x}}, \quad (14)$$
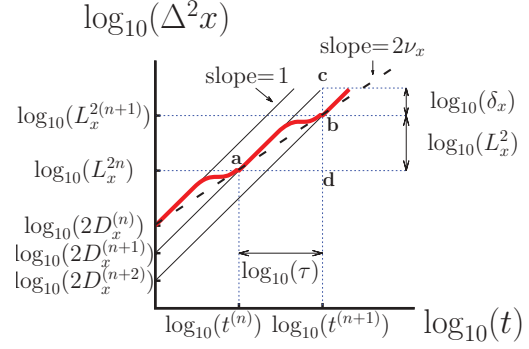

FIG. 3. (Color online) Schematic of the mean-square displacement in the x direction as a function of time, shown by the red (thick) curve. The length of the segment **bc** is $\log_{10}(2D_x^{(n)}) - \log_{10}(2D_x^{(n+1)}) = \log_{10}(\delta_x)$ because of Eq. (5). From the slopes ($= 1$) of the full straight lines (representing the normal diffusion behaviors $\Delta^2 x = 2D_x^{(n)} t$), one determines that the segments **ad** and **cd** have the same length or, equivalently, that $\log_{10}(\tau) = \log_{10}(L_x^2) + \log_{10}(\delta_x)$. The dashed straight line represents the global power law $\Delta^2 x \sim t^{2\nu_x}$ with $2\nu_x = \log_{10}(L_x^2)/\log_{10}(\tau)$. Thus, $\nu_x = (2 + \log_{10} \delta_x / \log_{10} L_x)^{-1}$. The mean-square displacement in the y direction exhibits an analogous behavior.

$$\nu_y = \frac{1}{2 + \frac{\log_{10} \delta_y}{\log_{10} L_y}}, \quad (15)$$

$$\tau_x = \delta_x L_x^2, \quad (16)$$

and

$$\tau_y = \delta_y L_y^2. \quad (17)$$

Note that even when $\nu_x \neq \nu_y$, the periods of the modulations coincide because of constraint (6), i.e.,

$$\tau_x = \delta_x L_x^2 = \frac{D_x^{(n)}}{D_x^{(n+1)}} L_x^2 = \frac{D_y^{(n)}}{D_y^{(n+1)}} L_y^2 = \delta_y L_y^2 = \tau_y, \quad (18)$$

where we have also used Eqs. (5) and (8). We call τ this period. From the equations above, the values of the period and the exponents are $\tau = 35$, $\nu_x = 0.4527$, and $\nu_y = 0.3090$.

Let us note that the average time to escape from a unit cell of the nth-generation is $t^{(n)} = \tau^n$, meaning that relations (10) and (11) hold for

$$\tau^n \lesssim t \lesssim \tau^{n+1}. \quad (19)$$

Then, when the RW leaves the initial region of size $L_x^n \times L_y^n$ to enter the next one of size $L_x^{n+1} \times L_y^{n+1}$, the length to width ratio L_x^n / L_y^n is increased by an anisotropic factor $a = L_x/L_y$ while the average time increases from t to τt. On the other hand, according to Eqs. (12) and (14), the corresponding mean-square displacements are related by $\Delta^2 x(\tau t) = L_x^2 \Delta^2 x(t)$ and $\Delta^2 y(\tau t) = L_y^2 \Delta^2 y(t)$. Therefore, in this transition, the ratio $\sqrt{\Delta^2 x / \Delta^2 y}$ is also increased by a factor a; i.e., the space explored by the RW grows with the same anisotropy as the substrate where the diffusion takes place.
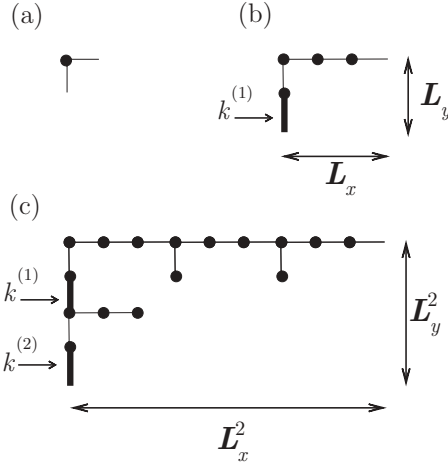
FIG. 4. The unit cells of model II. The zeroth, first, and second generations are shown in (a), (b), and (c), respectively. $L_x = 3$, and $L_y = 2$.

B. Model II

For this model, the unit cells for the zeroth, first, and second generations are shown in Fig. 4. The full self-affine substrate is here also obtained when the generation order goes to infinity. The linear sizes of the nth-generation unit cell are L_x^n and L_y^n with $L_x = 3$ and $L_y = 2$.

The diffusion of a single particle is analyzed as in model I. That is, we reformulate the two-dimensional RW problem on a one-dimensional array and compute the diffusion coefficients following the steady-state method [18].

For the nth generation, we obtain

$$D_x^{(n)} = \left(\tfrac{3}{4}\right)^n k^{(0)}, \quad \text{for } n = 0,1,2,\ldots, \tag{20}$$

and thus,

$$D_x^{(n)}/D_x^{(n+1)} = \delta_x = 4/3, \quad \text{for } n = 0,1,2,\ldots. \tag{21}$$

On average, the time to leave a nth-generation unit cell along the x direction becomes the same as that along the y direction if

$$D_y^{(n)} = \frac{k^{(0)}}{3^n}, \quad \text{for } n = 0,1,2,\ldots, \tag{22}$$

implying

$$D_y^{(n)}/D_y^{(n+1)} = \delta_y = 3, \quad \text{for } n = 0,1,2,\ldots. \tag{23}$$

The $k^{(i)}$ values, coming from Eq. (22), are again computed from Eq. (9) (with $L_x = 3$ and $L_y = 2$). Furthermore, in spite of the differences between model I and model II, we expect the qualitative behavior sketched in Fig. 3 to be valid for both models. Therefore, the RW exponents ν_x and ν_y and the period τ are given by Eqs. (14), (15), and (18) with the values $\nu_x = 0.4421$, $\nu_y = 0.2789$, and $\tau = 12$.

III. NUMERICAL RESULTS

To test the predictions outlined above, we perform standard RW Monte Carlo simulations on a nth-generation unit cell for each model. In model I (II), every RW starts at the center of symmetry of the cell (at the top-left-most site). The value of n is always chosen large enough to prevent the RWs from reaching the cell borders (the bottom and right cell borders) during the simulation. Working on this cell is thus equivalent to working with the full self-affine structure. In all simulations the hopping rate $k^{(0)}$ is set to 1/4, and the other $k^{(i)}$ values ($i \geqslant 1$) are obtained from Eq. (9). After every Monte Carlo step, the time is increased by $\Delta t = 1$.

With the numerical results of model I, in Fig. 5(a) we have plotted the mean-square displacement along the main directions. We see in these plots that both $\Delta^2 x(t)$ and $\Delta^2 y(t)$ are well described by modulated power laws. The upper and lower straight lines have slopes $2\nu_x$ and $2\nu_y$, respectively. They are drawn to guide the eyes, using the analytical values of the RW exponents. The log periodicity of the modulations can be better observed in Fig. 5(b) in which we have plotted $\Gamma_x = \log_{10}(\Delta^2 x/A_x t^{2\nu_x})$ and $\Gamma_y = \log_{10}(\Delta^2 y/A_y t^{2\nu_y})$ against t, using the same data as in Fig. 5(a). A_x (A_y) is a constant chosen to have the oscillations in the x (y) direction centered around 0.00 (0.05). The continuous lines are of the form $B \sin[2\pi \log_{10}(t)/\log_{10}(\tau) + \alpha]$, i.e., the first-harmonic approximation of a periodic function with period $\log_{10}(\tau)$ where B and α are fitted parameters and $\tau = 35$ (the above-given analytical period). It is clear from this figure that the theoretical predictions of Eqs. (14), (15), and (18) are consistent with the numerical findings.
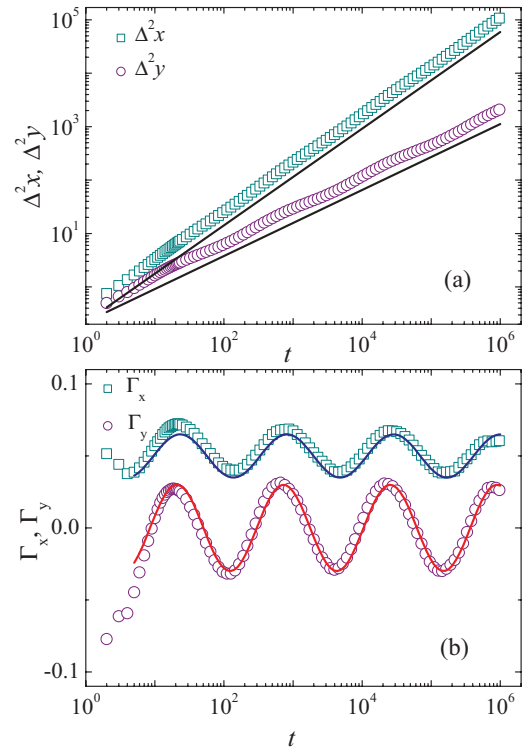

FIG. 5. (Color online) (a) The mean-square displacements $\Delta^2 x$ (green squares) and $\Delta^2 y$ (purple circles) as functions of time for model I. The upper straight line has a slope $2\nu_x$ with $\nu_x = 0.4527$ obtained from Eq. (14). The lower straight line has a slope $2\nu_y$ with $\nu_y = 0.3090$ obtained from Eq. (15). (b) Γ_x and Γ_y vs t for the same data. A_x and A_y are properly chosen constants. The curves represent the first-harmonic approximations $B_x \sin[2\pi \log_{10}(t)/\log_{10}(\tau) + \alpha]$ (blue, upper) and $B_y \sin[2\pi \log_{10}(t)/\log_{10}(\tau) + \beta]$ (red, lower). The period τ is given by Eq. (18). B_x, B_y, α, and β are fitted constants.
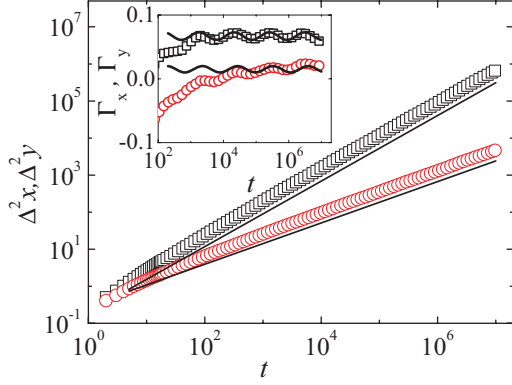
FIG. 6. (Color online) The mean-square displacement $\Delta^2 x$ (black squares) [$\Delta^2 y$ (red circles)] versus time for model II. The top straight line has a slope $2\nu_x = 0.8842$, and the lower straight line has a slope $2\nu_y = 0.5579$. Both exponents are obtained from Eqs. (14) and (15). The inset shows plots of Γ_x (black squares) and Γ_y (red circles) against t for the same data. The curves were obtained as in Fig. 5 with the period τ calculated from Eq. (18).

The corresponding numerical results for model II are shown in Fig. 6. Note that, also for this model, at long times, the mean-square displacement as a function of time is well described by modulated power laws. To better appreciate the log periodicity of the modulation, we have plotted Γ_x and Γ_y vs t in the inset of this figure. The fitting curves are of the form $D \sin[2\pi \log_{10}(t)/\log_{10}(\tau) + \alpha]$ with the analytical value $\tau = 12$. The agreement between analytical and numerical results is good too.

We consider now a substrate (model III) which consists of the full self-affine structure of model I but with the same hopping rate $k^{(0)}$ between any pair of connected NN sites. For this model, the average time to leave a nth-generation unit cell along the x direction is different from that along the y direction. It may occur that $L_x^n \lesssim \sqrt{\Delta^2 x(t)} \lesssim L_x^{n+1}$ and $L_y^m \lesssim \sqrt{\Delta^2 y(t)} \lesssim L_y^{m+1}$ for a given time t and $m \neq n$, in other words meaning that near t the RW behaves as in the nth-generation substrate regarding the x direction but as in the mth-generation substrate regarding the y direction. Thus, we cannot expect that the heuristic arguments in the previous section continue to be valid, and we have then to study the problem numerically.

The logarithm of the scaled mean-squared displacements (in the x and y directions) Γ_x and Γ_y are plotted in Fig. 7 as a function of the logarithm of time. The RW exponents $\nu_x = 0.4373$ and $\nu_y = 0.3859$ in this figure are fitted values. Let us note that ν_x is different from ν_y and that the data of Fig. 7 strongly suggest that the modulations have the same period τ in both directions. As expected, the numerical values of these parameters are not in agreement with Eqs. (14), (15), and (18). We would like to remark that if we used Eqs. (14) and (15) (with $\delta_x = 7/5$ and $\delta_y = 7/3$ resulting from the new hopping rates), we would get the RW exponents $\nu_x' = 0.4527$ and $\nu_y' = 0.3609$, which, in turn, would lead to the periods $\tau_x' = L_x^{1/\nu_x'} = 35$ and $\tau_y' = L_y^{1/\nu_y'} = 21$, different from each other (see the caption of Fig. 3 for the equation $\tau = L^{1/\nu}$). Note that the numerical value of $\nu_x = 0.4373$ ($\nu_y = 0.3859$)
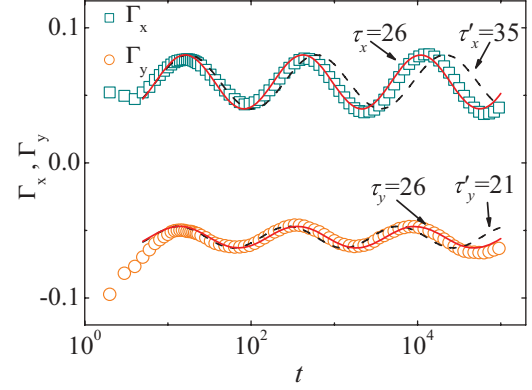

FIG. 7. (Color online) Scaled mean-square displacements for model III. Plot of Γ_x (green squares) and Γ_y vs t (orange circles), using numerical data. (C_x and C_y are properly chosen constants; see the text.) The full lines represent the first-harmonic approximations $A_x \sin[2\pi \log_{10}(t)/\log_{10}(\tau) + \alpha]$ (upper) and $A_y \sin[2\pi \log_{10}(t)/\log_{10}(\tau) + \beta]$ (lower) of Γ_x and Γ_y, respectively. Here, $\tau = 26$, A_x, A_y, α, and β are fitted constants. The upper dashed line represents the first-harmonic approximation of Γ_x with period $\tau_x' = 35$. The lower dashed line represents the first-harmonic approximation of Γ_y with period $\tau_y' = 21$.

is smaller than ν_x' (larger than ν_y'), and the numerical value period τ is in the range $[\tau_y', \tau_x']$ ($\tau \cong 26$). For model III, Eqs. (10), (11), and (19) do not hold because, on average, the RW reaches the top or bottom border of the nth-generation unit cell before reaching the right or left border of the same cell. In the case of model I, this is avoided by properly modifying some hopping rates in every generation. The diffusion spread in the y direction is thus slowed down [$k^{(n)} < k^{(n-1)}$, see Eq. (9)], and the horizontal and vertical cell borders are, on average, reached simultaneously.

IV. DISCUSSION AND CONCLUSIONS

We have studied single-particle diffusion on a finitely ramified self-affine structure in two dimensions. For a special kind of model for which the ratio between the x and y mean-square displacements matches the structure anisotropy, we argue that the RW exponent in the x direction ν_x is different from that in the y direction ν_y and that the global subdiffusive behavior is modulated by log-periodic oscillations with a period τ which does not depend on the direction. The arguments employed in this work allow the main properties of the particle mean-square displacement to be obtained as a function of model parameters. Because our arguments are somehow heuristic, Monte Carlo simulations using two models, I and II, were also carried out. The numerical results confirm our theoretical predictions.

For the rest of the self-similar systems, our conclusions are more limited due to the lack of suitable analytical methods and that the RW explores the space with an anisotropy different from that of the substrate. The results of the Monte Carlo simulations performed using one of these models (III) show (within the accuracy of the simulation) that also in this case $\nu_x \neq \nu_y$ and that the RW mean-square displacement

is modulated by log-periodic oscillations with an isotropic period. However, we cannot guarantee that this behavior will hold in the limit of an arbitrarily long time; that is why we have introduced models I and II. Let us finally note that the extension of our analytical results to other values of L_x and L_y is straightforward.

[1] S. Alexander and R. Orbach, J. Physique Lett. **43**, 625 (1982); R. Rammal and G. Toulouse, *ibid*. **44**, 13 (1983); G. H. Weiss and S. Havlin, Philos. Mag. B **56**, 941 (1987); D. Ben-Avraham and S. Havlin, *Diffusion and Reactions in Fractals and Disordered Media* (Cambridge University Press, Cambridge, 2000); S. Havlin and D. Ben-Avraham, Adv. Phys. **36**, 695 (1987); J.-P. Bouchaud and A. Georges, Phys. Rep. **195**, 127 (1990).

[2] W. Woess, *Random Walks on Infinite Graphs and Groups* (Cambridge University Press, Cambridge, 2000); P. J. Grabner and W. Woess, Stochastic Process. Appl. **69**, 127 (1997); B. Krön and E. Teufl, T. Am. Math. Soc. **356**, 393 (2003); L. Acedo and S. B. Yuste, Phys. Rev. E **63**, 011105 (2000); M. A. Bab, G. Fabricius, and E. V. Albano, Europhys. Lett. **81**, 10003 (2008); J. Chem. Phys. **128**, 044911 (2008); A. L. Maltz, G. Fabricius, M. A. Bab, and E. V. Albano, J. Phys. A **41**, 495004 (2008); S. Weber, J. Klafter, and A. Blumen, Phys. Rev. E **82**, 051129 (2010).

[3] L. Padilla, H. O. Mártin, and J. L. Iguain, Europhys. Lett. **85**, 20008 (2009).

[4] L. Padilla, H. O. Mártin, and J. L. Iguain, Phys. Rev. E **82**, 011124 (2010).

[5] J. Bernasconi and W. R. Schneider, J. Stat. Phys. **30**, 355 (1983); D. Stauffer and D. Sornette, Phys. A (Amsterdam, Neth.) **252**, 271 (1998); D. Stauffer, *ibid*. **266**, 35 (1999); Z. Yu-Xia, S. Jian-Ping, Z. Xian-Wu, and J. Zhun-Zhi, *ibid*. **350**, 163 (2005).

[6] Y. Huang, H. Saleur, C. Sammis, and D. Sornette, Europhys. Lett. **41**, 43 (1998); H. Saleur, C. Sammis, and D. Sornette, J. Geophys. Res. **101**, 17661 (1996).

[7] A. Krawiecki, K. Kacperski, S. Matyjaśkiewicz, and J. A. Hołyst, Chaos, Solitons Fractals **18**, 89 (2003).

[8] B. Kutnjak-Urbanc, S. Zapperi, S. Milosevic, and H. E. Stanley, Phys. Rev. E **54**, 272 (1996); R. F. S. Andrade, *ibid*. **61**, 7196 (2000); M. A. Bab, G. Fabricius, and E. V. Albano, *ibid*. **71**, 036139 (2005); H. Saleur and D. Sornette, J. Phys. I **6**, 327 (1996).

[9] D. Sornette, A. Johansen, A. Arneodo, J. F. Muzy, and H. Saleur, Phys. Rev. Lett. **76**, 251 (1996).

[10] Y. Huang, G. Ouillon, H. Saleur, and D. Sornette, Phys. Rev. E **55**, 6433 (1997).

[11] D. Sornette, A. Johansen, and J.-P. Bouchaud, J. Phys. I **6**, 167 (1996); N. Vanderwalle, P. Boveroux, A. Minguet, and M. Ausloos, Phys. A (Amsterdam, Neth.) **255**, 201 (1998); N. Vanderwalle and M. Ausloos, Eur. J. Phys. B **4**, 139 (1998); N. Vanderwalle, M. Ausloos, Ph. Boveroux, and A. Minguet, *ibid*. **9**, 355 (1999).

[12] B. Doucot, W. Wang, J. Chaussy, B. Pannetier, R. Rammal, A. Vareille, and D. Henry, Phys. Rev. Lett. **57**, 1235 (1986).

[13] D. Sornette, Phys. Rep. **297**, 239 (1998).

[14] P. Meakin, *Fractals, Scaling and Growth Far From Equilibrium* (Cambridge University Press, Cambridge, 1998).

[15] P. Meakin and F. Family, Phys. Rev. A **34**, 2558 (1986).

[16] C. Evertsz, Phys. Rev. A **41**, 1830 (1990).

[17] J. P. Bouchaud, E. Bouchaud, G. Lapasset, and J. Planès, Phys. Rev. Lett. **71**, 2240 (1993).

[18] C. M. Aldao, J. L. Iguain, and H. O. Mártin, Surf. Sci. **366**, 483 (1996).